Proceedings of CONF-FMCE 2025 Symposium: Semantic Communication for Media Compression and Transmission
DOI: 10.54254/2755-2721/2025.GL27340

The Combination of Knee Limiting Braces and Origami Structures

Mingkun Zhao[1*], Yutong Zhou[2], Shiyu Ren[2]

[1]School of Future Technology, Tianjin University, Tianjin, China
[2]Hang Zhou Wickham School, Hangzhou, China
**Corresponding Author. Email: zmk123450@163.com*

Abstract. In ACL postoperative rehabilitation, standardized knee motion-limiting braces often fail to adapt to individual leg morphology differences, which hinder rehabilitation and user experience. To address these issues, this study aims to propose a dynamically conforming arc-Miura fold-inspired design to replace conventional skin-fitting straps. The research first elaborates on the overall design concept, highlighting two key advantages of the arc-Miura structure: improved anatomical conformity (adapting to heterogeneous skin surfaces via controlled deformation) and mechanical efficiency (evenly distributing forces through tessellated geometry). Subsequently, the interface design between the Miura fold and the rigid brace frame is detailed, including a U-shaped groove for smooth kinematic transition and a triangular linkage mechanism with modular scalability and fold-driven actuation. The motion mechanism of the arc-Miura structure is systematically analyzed: based on a single input parameter (folding angle ρA1B1), the correlation formulas between ρA1B1 and key parameters (arc radius Ri, structural span L, cumulative angle n·x) are derived, and the ring-forming characteristics in the fully folded state are explored, leading to the adoption of a semi-arc structure to avoid excessive overlap. Parameter optimization is conducted by investigating the influence of core parameters (a1, a2, αI1, αI1') on crease distribution, and constraint conditions for thigh and calf adaptation are established. Through algorithm optimization, structural parameters suitable for the thigh and calf are obtained, with their performance ranges meeting ergonomic requirements. This study systematically explores the integration of origami structures with knee-limiting braces, addressing the limitations of conventional braces in dynamic conformity and mechanical efficiency. Through design, analysis, optimization, and prototype fabrication, it provides a novel solution for improving knee brace ergonomics, demonstrating the feasibility of origami engineering in optimizing wearable device performance.

Keywords: Knee limiting brace, Arc-Miura origami, Motion mechanism, Parameter optimization, Skin-fit performance, Wearable device

1. Introduction

In ACL postoperative rehabilitation, the core function of a knee motion-limiting brace is to stabilize the joint, restrict abnormal movement, and ensure ligament recovery. However, most mainstream

© 2026 The Authors. This is an open access article distributed under the terms of the Creative Commons Attribution License 4.0 (https://creativecommons.org/licenses/by/4.0/).

DOI: 10.54254/2755-2721/2025.GL27340

braces are mass-produced, standardized products. Although some come with elastic straps for adjusting the tightness, significant individual differences in leg morphology (such as thigh circumference, kneecap morphology and lower limb alignment) make it difficult for standardized braces to fully conform to every patient's leg contour [1].

This lack of adaptability not only may allow unintended twisting inside the brace, compromising its motion-limiting effectiveness and potentially hindering rehabilitation, but also poses usability challenges. Without professional guidance, patients often struggle to achieve a snug fit when self-adjusting the brace, leading to frequent slippage. This reduces convenience and user-friendliness.

To address these issues—improving brace adaptability to diverse leg shapes, effectively preventing internal twisting, and enhancing decline problem to minimize slippage—we propose integrating the Arc-Miura origami structure into brace design. Leveraging its unique folding mechanics and adjustable morphological adaptability, the Arc-Miura structure could optimize brace-leg contact, improve constraint stability and ease of wear, thereby resolving twisting and slippage problems while boosting rehabilitation support.

As for what it is the Arc-Miura, it is a highly efficient space-saving folding technique invented in the 1970s by Japanese aerospace engineer Kōryō Miura. Below are the key milestones in its development: Miura drew inspiration from Japanese origami, particularly the application of creasing pattern geometry. While working at Japan's Institute of Space and Astronautical Science (ISAS), he sought solutions for compact storage of large structures like satellite solar panels. The Arc-Miura have some features, such as, enhanced durability, space optimization, high material adaptability. The Arc-Miura have some applications. For example, in aerospace, artificial satellite antenna and solar panel, and in industry like car airbags, heart stents and so on [2].

2. Design

2.1. Preliminary ideas for knee brace design

To enhance the skin-fit performance of the knee brace, this study proposes replacing the conventional skin-fitting strap (Figure 1(a)) with a dynamically conforming Miura-fold-inspired arc structure (Figure 1(b)). This origami-derived design enables programmable folding along curvilinear paths (Figure 1(c)), offering two key advantages:

(1) Improved Anatomical Conformity: The Miura structure adapts to heterogeneous skin surfaces via controlled deformation, reducing localized pressure points.

(2) Mechanical Efficiency: The tessellated geometry distributes tensile/compressive forces evenly across the strap-brace interface.

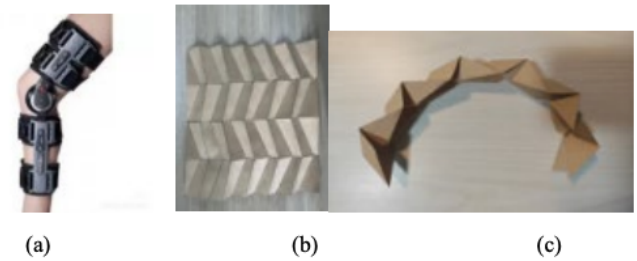


Figure 1. (a) Traditional knee limiting brace and (b) Arc-Miura origami structure and (c) Folded Arc-Miura

DOI: 10.54254/2755-2721/2025.GL27340

2.2. Interface design between Miura fold and rigid brace frame

The interface between the Miura fold and the rigid brace frame incorporates a U-shaped groove (Figure 2 (a)-2.2(b), top/side view) for smooth kinematic transition. A triangular linkage mechanism bridges the Miura fold's terminal edge to the U-groove, featuring:

(1) Modular Scalability: Composed of repeatable triangular units (Figure 2(c)) with telescopic joints for adjustable arc curvature.

(2) Fold-Driven Actuation: Unit fabrication follows a prescribed crease pattern (Figure 3), enabling synchronized folding motion.

This hybrid design (foldable arc + rigid support) demonstrates how origami engineering can optimize wearable device ergonomics while maintaining structural integrity.

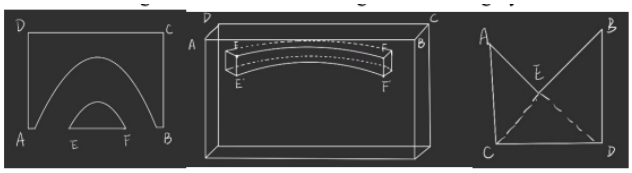


Figure 2. (a) Top view of U-shaped groove and (b) Side view of U-shaped groove and (c) Repeatable triangular units

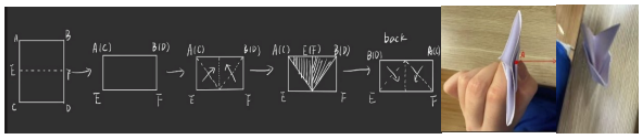


Figure 3. Folding steps for repeatable triangular units

3. Analysis

3.1. The motion mechanism of Arc-Miura

3.1.1. Design parameters of the Arc-Miura pattern

The Miura pattern is achieved by repeating a unit cell geometry along two axes on the same plane. The unit cell geometry consists of four identical quadrangle defined by four parameters, a1, a2, αI1 and αI1' (Figure 4).

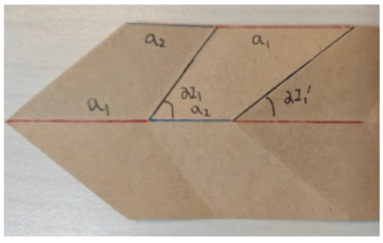


Figure 4. A picture of a single Arc-Miura unit cell with parameters included

DOI: 10.54254/2755-2721/2025.GL27340

3.1.2. Analysis of the motion mechanism of Arc-Miura based on a single input parameter

3.1.2.1. Selection and basis of input parameters

The Arc-Miura origami structure exhibits a single-degree-of-freedom characteristic, meaning its folding motion can be accurately described by a single independent parameter. As shown in Figure 5, this study selects the angle ρA1B1 between the normal vector OM of plane ABDC and the normal vector O‘M’ of plane EFDC as the input parameter. This angle can intuitively reflect the folding degree of the structure: when the structure is in a fully unfolded state, ρA1B1 approaches the initial angle (0 degrees); as folding proceeds, the angle changes continuously until reaching the fully folded state (180 degrees). By selecting ρA1B1 as the input, the response laws of other structural parameters during the folding process can be systematically explored through controlling a single variable.

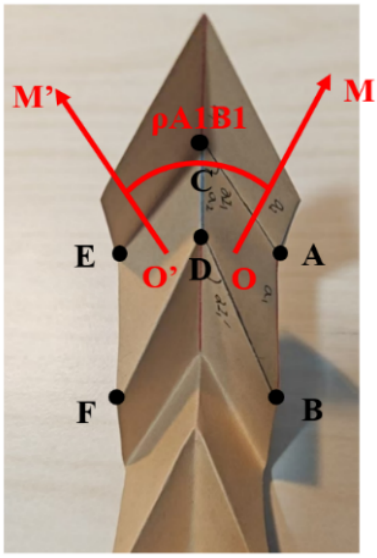


Figure 5. Representation of the input parameter on the model

3.1.2.2. Extraction of geometric features and derivation of formulas

Since the creases of the Arc-Miura structure are always coplanar (lying in the same plane), this study adopts geometric mapping and feature analysis methods: by observing the morphology of the physical object, i.e., extracting the crease distribution from the physical object as shown in Figure 6, the geometric information in Figure 7 is obtained. Specifically, the red line a1 and blue line a2 represent the creases; the green line l denotes the unit span; Ri is the radius of the arc; x is the central angle of a single unit cell; L stands for the overall structural span; and n*x represents the cumulative angle of multiple units. Based on the planar geometric relationships and combined with the input parameter ρA1B1, the correlation formulas between ρA1B1 and other parameters (such as the radius Ri of the arc formed by the creases, the single-cell span l, and the overall structural span L) are derived.

DOI: 10.54254/2755-2721/2025.GL27340

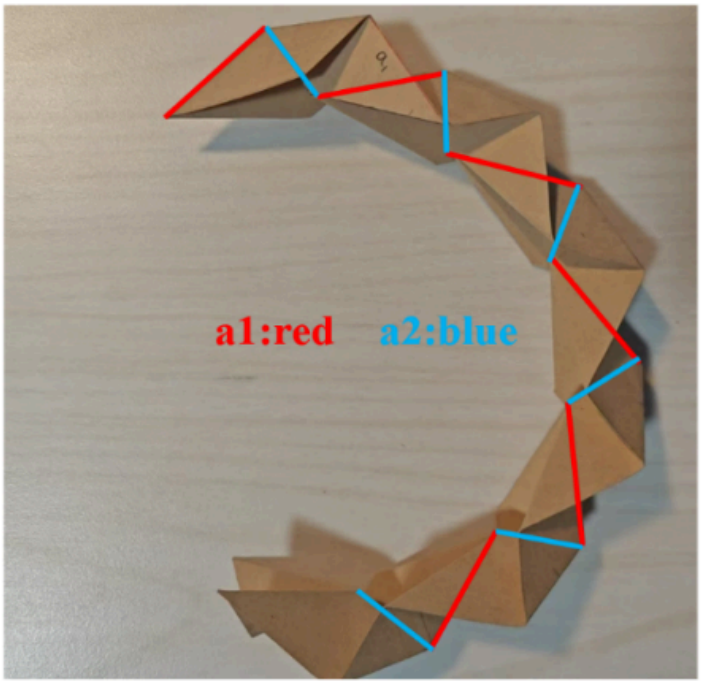


Figure 6. Crease distribution in the side view

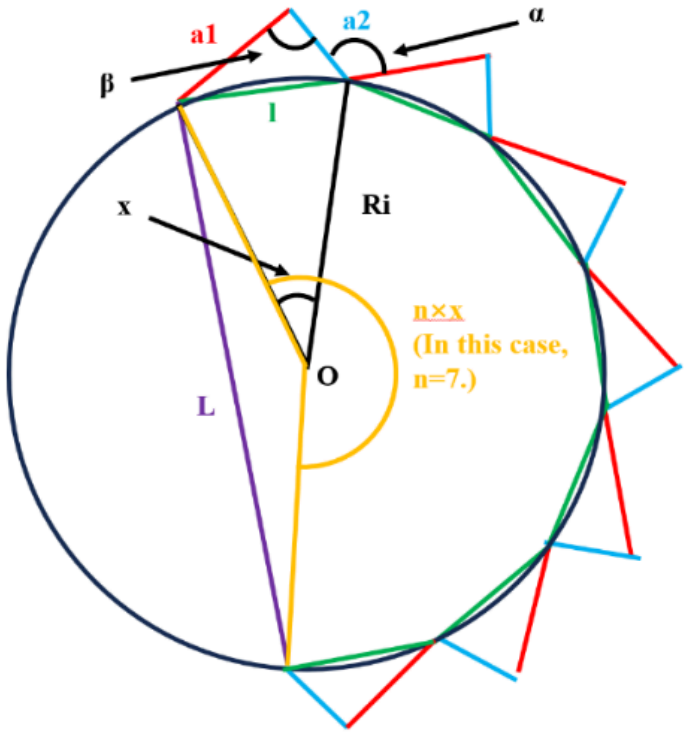


Figure 7. Extracted geometric features

Eqs. (1) to (8) represent the relationships among all parameters of the Arc-Miura parametric model [3,4].

DOI: 10.54254/2755-2721/2025.GL27340

$$R_i = \sqrt{\frac{a_1^2+a_2^2-2a_1a_2\cos\beta}{2(1-\cos(\alpha-\beta))}} \tag{1}$$

$$l = \sqrt{a_1^2 + a_2^2 - 2a_1a_2\cos\beta} \tag{2}$$

$$L = 2R_i \sin\frac{nx}{2} \tag{3}$$

$$\sin\frac{x}{2} = \frac{l}{2R_i} \tag{4}$$

$$\cos\beta = -\cos^2(\pi-\alpha_{I1}) - \sin^2(\pi-\alpha_{I1})\left(\frac{1-K_1^2}{\cos\rho_{A1B1}-K_1} - K_1\right) \tag{5}$$

$$K_1 = \frac{1+\cos\alpha_{I1}^2}{\sin\alpha_{I1}^2} \tag{6}$$

$$\cos\alpha = -\cos^2\left(\pi-\alpha_{I1}^{'}\right) - \sin^2\left(\pi-\alpha_{I1}^{'}\right)\left(\frac{1-K_2^2}{\cos\rho_{A1B1}-K_2} - K_2\right) \tag{7}$$

$$K_2 = \frac{1+\cos\alpha_{I1}^{'2}}{\sin\alpha_{I1}^{'2}} \tag{8}$$

3.1.3. Study on ring formation of Arc-Miura under full folding

3.1.3.1. Research background and methods

Based on the clarified motion mechanism of the Arc-Miura origami structure (Section 3.1.2), this study further explores its ring-forming characteristics in the fully folded state.

First, it is necessary to clarify the value logic of the benchmark parameters a1, a2, αI1, and αI1'. Since the creases of the Arc-Miura origami structure are coplanar and the geometric features of the unit cells (elements) are uniform (each unit has the same size and shape), the parameters in this study are determined through the extraction of geometric features and the derivation of constraint relationships:

(1) The geometric constraint structure of creases and unit cells is composed of n unit cells arranged periodically. Each unit cell contributes 2 creases, so the total number of creases is 2n. Based on the theorem of the sum of interior angles of a polygon, the closed contour formed by the creases can be regarded as a "polygonalized" structure, and the sum of its interior angles satisfies:

$$S = (2n-2)\times 180^\circ \tag{9}$$

(2) Constraint relationship of angle parameters In the fully folded and ring-formed state, the angle parameters αI1 and αI1' of the unit cell have strict constraints with the geometric angles α and β formed by the creases. Based on the coplanarity of the creases and the requirement of folding closure, the relationship between the geometric angles and the design parameters is derived as follows:

DOI: 10.54254/2755-2721/2025.GL27340

$$\begin{cases} \alpha = \pi - 2\alpha_{I1}^{'} \\ \beta = \pi - 2\alpha_{I1} \end{cases} \tag{10}$$

(3) Derivation of the ring formation condition When the structure is fully folded into a ring, the cumulative angles of all unit cells must satisfy the closure constraint. Combined with the angular relationship of the unit cells, the core condition for ring formation is:

$$n \cdot \left(\alpha_{I1} - \alpha_{I1}^{'}\right) = 180^{\circ} \tag{11}$$

The physical meaning of this condition is that the cumulative angular difference of the n unit cells must exactly compensate for the phase difference required for planar closure, enabling the two ends of the structure to interlock and form a complete ring. In this study, the number of unit cells is preset as n = 10, and based on the ring formation condition, the reference parameters are deduced inversely, i.e., the difference between αI1 and αI1' is 18°.

3.1.3.2. Variation laws of key parameters

Based on the previous analysis, the test parameters are selected as n=10, a1=10, a2=7, αI1=70, and αI1'=52. With the folding angle ρA1B1 (ranging from 0° to 180°, corresponding to the process of the structure from fully unfolded to fully folded) as the input variable, parametric analysis is carried out using MATLAB. The focus is placed on studying the variation laws of key parameters such as the structural span L with ρA1B1, so as to reveal the ring formation process and parameter adaptability.

Through MATLAB simulation calculations, the variation curve of the structural span L with the folding angle ρA1B1 is obtained (Figure 8).

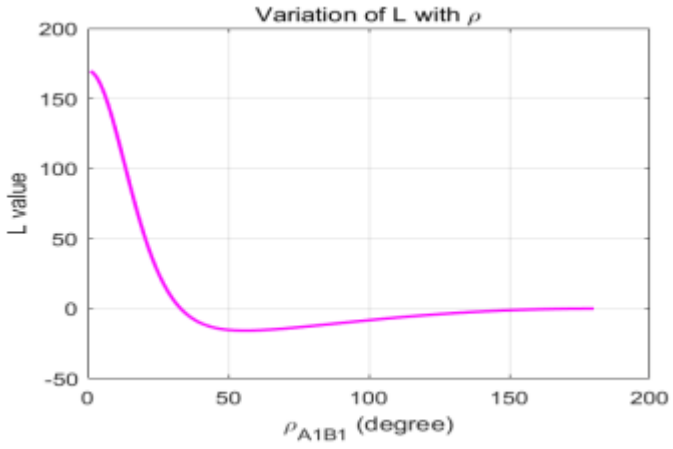


Figure 8. Curve of L versus ρA1B1

The analysis reveals that as the Arc-Miura structure transitions from a fully unfolded state (i.e., as ρA1B1 gradually increases from 0°), the structural span L undergoes a non-linear change. When ρA1B1 reaches approximately 30°, L becomes zero for the first time, indicating that the two ends of the origami structure have met, initially showing a "pre-ring formation" trend. As ρA1B1 continues to increase, within the range of approximately 30° to 50°, the absolute value of the negative L

DOI: 10.54254/2755-2721/2025.GL27340

further increases, reflecting that the two ends of the structure continue to "over-fold" after meeting, forming an "over-ring" conFigureuration. When ρA1B1 exceeds 50°, the absolute value of the negative L gradually decreases until ρA1B1 reaches 180° (the origami structure is fully folded), at which point L returns to zero, and the structure finally engages front and back to form a closed loop. Keeping n constant and the difference between αI1 and αI1' unchanged, with a1 and a2 taking random values, the results are shown in Figure 9.

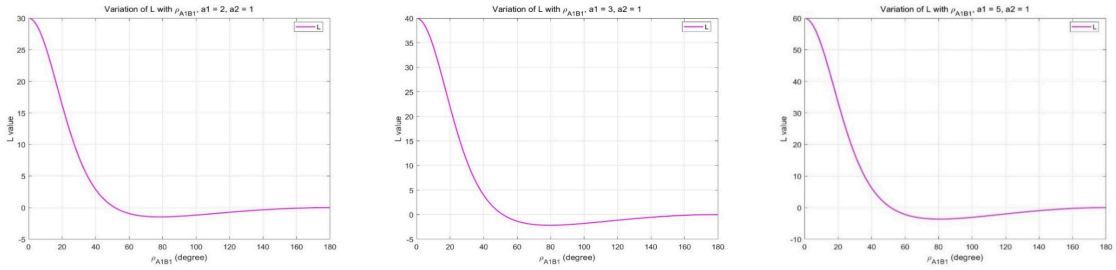


Figure 9. Curves of L versus ρA1B1 under various parameters

Studies have shown that if the Arc-Miura structure is required to form a closed ring when fully folded, its folding process must be accompanied by an "excessive overlap" (i.e., "over-ring") phenomenon. Before reaching the final ring state, the structure will first go through an unstable stage where both ends overlap excessively, and then gradually adjust to the closed form.

This process is in significant contradiction with the design goal of "adapting to the leg curvature and achieving dynamic size adjustment": the curvature change of the leg surface is continuous and smooth, requiring the structure to fit in real time with limb movement. However, "excessive overlap" will lead to a sudden increase in local rigidity of the structure and lag in deformation response, which cannot meet the comfort and dynamic adaptation requirements during wearing.

Therefore, to avoid the above problems, it is necessary to adjust the structural design strategy—using a semi-arc structure instead of a complete ring structure. The semi-arc structure can avoid the excessive overlap stage required for forming a closed ring by controlling the folding range, while retaining sufficient deformation freedom to adapt to changes in leg curvature, thus better meeting the design requirements.

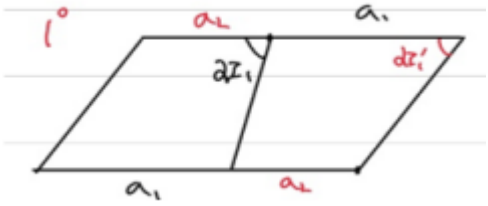
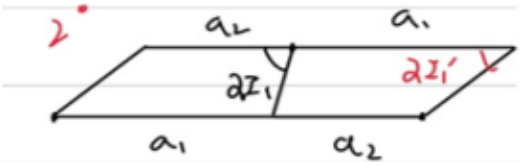
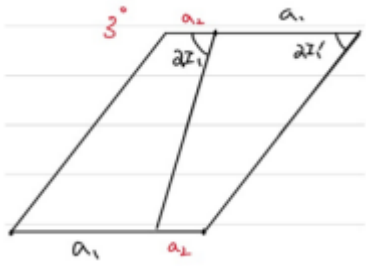
3.2. Distribution of internal creases under different Arc-Miura parameters

Crease distribution is a key factor affecting the fit and comfort of the Arc-Miura structure with the leg. Since the structure needs to be attached to the human leg, a higher density of internal creases enables it to better adapt to the curved contour of the leg during the folding process, reducing local pressure and thus improving the body's comfort. Therefore, this section focuses on exploring the influence of different values of core parameters a1, a2, αI1, and αI1' on the internal crease distribution of the Arc-Miura structure, and analyzes the direction of parameter optimization based on experimental results.

For the experimental design, to clarify the impact of a single parameter change on crease distribution, this study adopts the control variable method, fixes the values of a1 and αI1, and designs three groups of comparative samples (Table 1):

DOI: 10.54254/2755-2721/2025.GL27340

Table 1. Three groups of comparative samples: first row (Control group): adopting benchmark parameters; second row (Sample 2): only reducing the value of αI1' (other parameters are consistent with the control group); third row (Sample 3): only reducing the value of a2 (other parameters are consistent with the control group)

A sketch of a cell	a1	a2	αI1	αI1’
	3cm	2cm	60°	45°
	3cm	2cm	60°	30°
	3cm	1cm	60°	45°

It should be specifically noted that a single unit cell of the Arc-Miura structure is jointly defined by four core parameters: a1, a2, αI1, and αI1'. These four parameters have symmetry in geometric significance—that is, a1 and a2 are merely different in name, and their influences on crease distribution are symmetric; similarly, αI1 and αI1' are also only different in name, and the laws of their individual changes on crease characteristics are completely consistent. Based on this symmetry, when exploring the influence of a single parameter change, there is no need to design control groups for the four parameters respectively. Therefore, in this study, only a2 and αI1' are selected as variables to design comparative experiments, and the laws of the other two parameters when changing individually can be inferred from the results.

After making physical models of the three groups of samples, they are folded to the same degree of folding (the folding state is unified by controlling the value of ρA1B1), and the distribution density of internal creases is observed and compared (Figure 10).

DOI: 10.54254/2755-2721/2025.GL27340

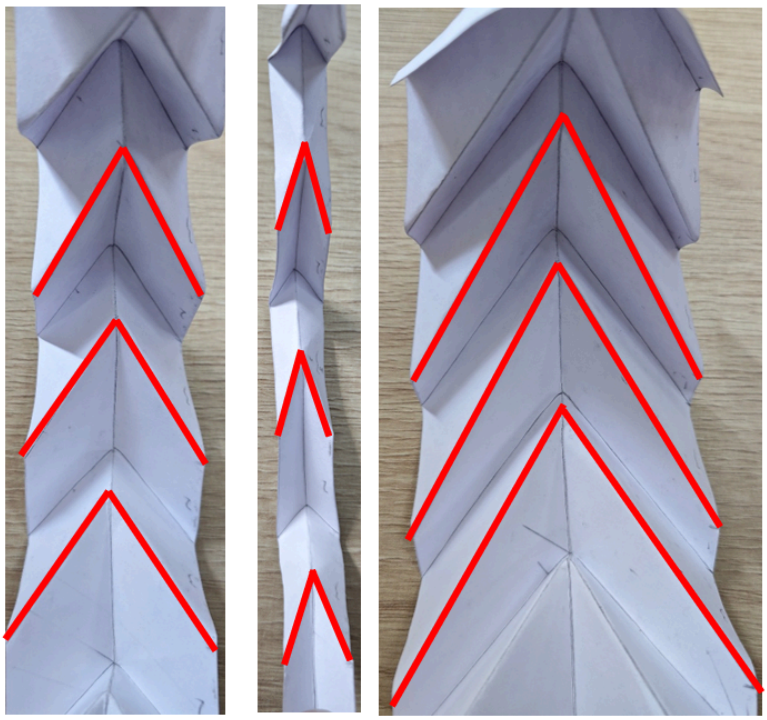


Figure 10. Internal crease distribution under three designs (creases are marked in red)

There are significant differences in the crease distribution among the three groups of samples:

Control group: The crease distribution density is at a medium level, with uniform crease spacing but not reaching a dense state; Sample 2 (with reduced αI1'): The crease density is significantly lower than that of the control group, with increased crease spacing, resulting in insufficient wearing comfort; Sample 3 (with reduced a2): The crease density is significantly higher than that of the control group, with more closely arranged creases.

Further analysis shows that when a1 and αI1 remain unchanged, the influence of parameter changes on crease density presents a regular pattern: reducing a2 will increase the crease density, while reducing αI1' will decrease the crease density. This pattern is closely related to the geometric mechanism of crease formation: crease density essentially reflects the structure's ability to distribute deformation during folding. The higher the density, the more dispersed the deformation, and the better the fit. Thus, on the premise of ensuring the folding performance of the structure, the delicacy of crease distribution can be maximized, thereby improving wearing comfort.

3.3. Specific parameter selection

To enable the Arc-Miura origami structure to be suitable for wearing on the human leg, it is necessary to formulate constraint conditions, respectively, according to the physiological and geometric characteristics of the thigh and calf. The human leg (thigh and calf) presents a specific curved contour and range of motion. The span L, arc radius Ri, and unit angle accumulation n*x of the origami structure must match the leg size and movement requirements to ensure fit and comfort during the folding process. By investigating ergonomic data and leg surface features, the constraint conditions are established as follows:

(1) Thigh adaptation constraints

• Angle accumulation constraint: Unit angle accumulation $n \cdot x \in [180^\circ, 250^\circ]$;

DOI: 10.54254/2755-2721/2025.GL27340

• Arc radius constraint: Arc radius $R_i \in [7\text{ cm}, 9.5\text{ cm}]$;
• Structural span constraint: Overall span $L \in [14\text{ cm}, 19\text{ cm}]$.
(2) Calf adaptation constraints
• Angle accumulation constraint: Unit angle accumulation $n \cdot x \in [180^\circ, 250^\circ]$;
• Arc radius constraint: Arc radius $R_i \in [4.5\text{ cm}, 7\text{ cm}]$;
• Structural span constraint: Overall span $L \in [8\text{ cm}, 11\text{ cm}]$.

Through algorithm optimization based on these constraint conditions, the Arc-Miura structure parameters adapted to the thigh are obtained:

a1 = 4.56 cm, a2 = 2.65 cm, αI1 = 70.80°, αI1' = 52.54°.

Similarly, the optimized structural parameters for calf adaptation are obtained as follows:

a1 = 3.14 cm, a2 = 2.03 cm, αI1 = 71.77°, αI1' = 51.09°.

Substituting the optimized parameters into the kinematic model of the Arc-Miura structure (the relationships between L, Ri, n*x and ρA1B1 derived in Section 3.1), the range for the thigh is:

n*x range: 182.66° - 220.36°, Ri range: 7.40cm - 9.49cm, L range: 14.62cm - 18.56cm

The range for the calf is:

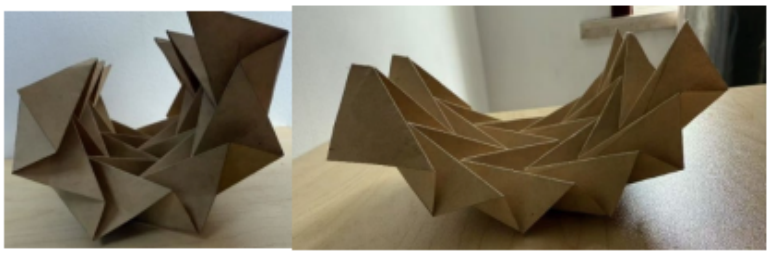
n*x range: 206.74° - 248.52°, Ri range: 4.76cm - 6.09cm, L range: 8.46cm - 10.99cm

All meet the requirements.

4. Real model

4.1. Origami structure design for the thigh and calf sections

Based on kinematic calculations (Section 3.3), the thigh and calf models were fabricated using thick hard cardboard (thickness: 2.5 mm) to achieve optimal skin conformity. As shown in(Figures 11 (a)-4.1(b)), Laser-cut contours match anthropometric data (thigh circumference: 48±2 cm, calf: 36±2 cm).



(a) (b)

Figure 11. (a) Origami schematic model of the thigh part and (b) Origami schematic model of the calf part

4.2. Lockable bracket system

The load-bearing framework (Figure 12) was constructed from wood, with critical dimensions (Table 2) [5]:

DOI: 10.54254/2755-2721/2025.GL27340

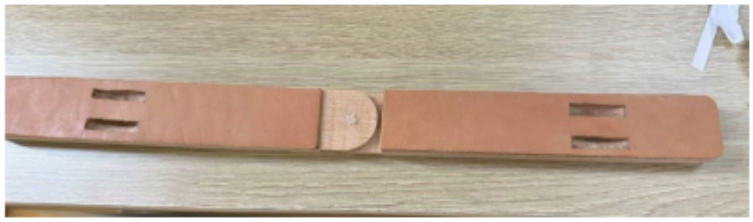


Figure 12. The load-bearing framework

Table 2. Key dimensions of the frame

Component	Length (cm)	Key Feature
Thigh bracket	24.0	U-groove spacing: 3.5±0.1 cm
Calf bracket	22.0	Rotational shaft: Φ3.5 cm

The manufacturing process involved:
(1) U-Groove Fabrication(Figure 13):
Milled 5-mm deep channels with 120° flank angles;
Leather-clad surfaces (0.8-mm bovine hide);
Dual 4-mm diameter penetration holes for Miura-structure integration.



Figure 13. U-Groove

(2) Rotation Mechanism(Figure 14):
Implemented a quadrant-locking system and mortise and tenon joints



Figure 14. Rotation mechanism

DOI: 10.54254/2755-2721/2025.GL27340

4.3. Triangular linkage assembly

(1) Modular Fabrication:

Made according to the design drawing, it has one open end and one closed end, and can be connected to the triangular unit structure (Figure 15(a)). The interlocking tolerance is +0.1/-0.05 mm to ensure buckling-free engagement [6,7].

(2) Kinematic Integration:

• Sequential connection via apex-groove coupling;
• Symmetrical mounting to Miura arcs (Figure 15(b));
• Final fixation through reverse-buckling with nylon retention rings (Figure 16).



(a) (b)

Figure 15. (a) Triangular unit structure and (b) Installation schematic diagram

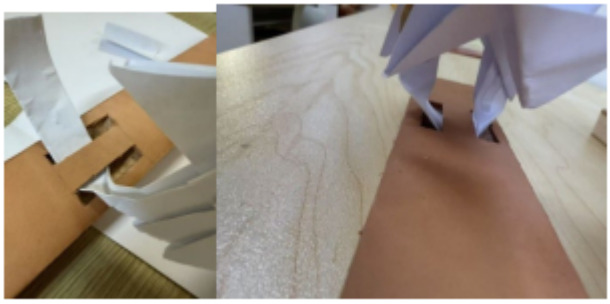


Figure 16. Fixation schematic diagram

4.4. Overall model

By integrating the aforementioned component models, the overall model is finally obtained. Figures 17(a)-4.7(c) show the appearance of the overall model, among which Figure 17(b) presents the overall structural characteristics from the perspective of the thigh, and Figure 17(c) presents the overall structural characteristics from the perspective of the calf. These Figures reflect the assembly relationship of each component and the overall configuration. Figure 17(d), on the other hand, shows the image of the model after being worn.

DOI: 10.54254/2755-2721/2025.GL27340

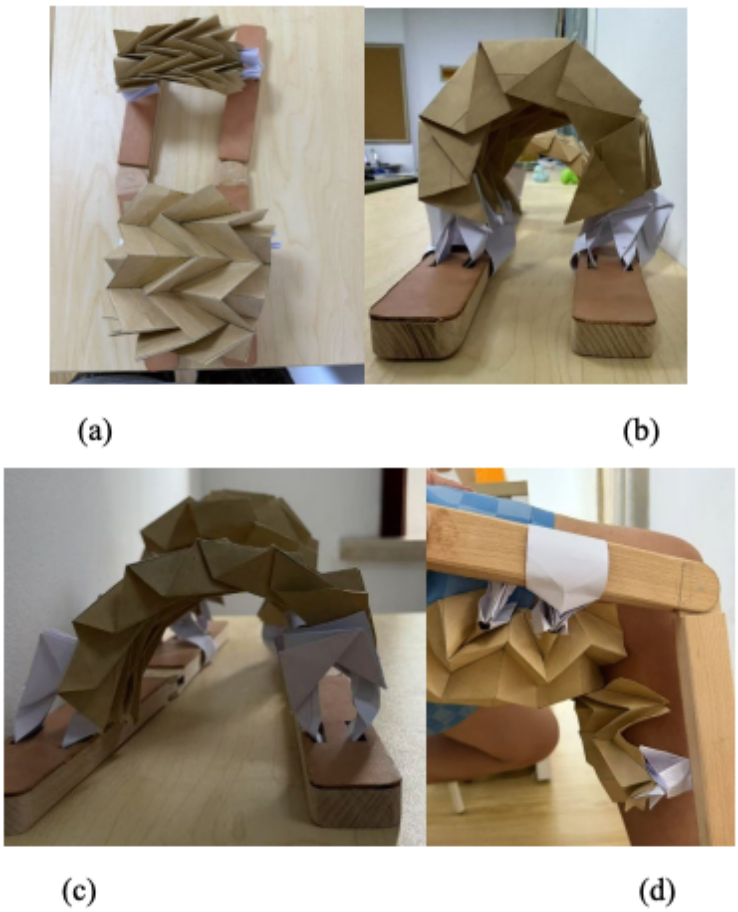


Figure 17. (a) Complete model and (b) View of the side of the thigh and (c) View of the side of the calf and (d) Wearing diagram

5. Conclusion

This study systematically explores the integration of origami structures with knee-limiting braces, aiming to address the limitations of conventional braces in dynamic conformity and mechanical efficiency. Through design, analysis, optimization, and prototype fabrication, the following key conclusions are drawn:

(1) Innovative Design of Arc-Miura Structure: By replacing traditional skin-fitting straps with a dynamically conforming Arc-Miura fold-inspired structure, the brace achieves two critical improvements. First, it enhances anatomical conformity, enabling adaptive deformation to heterogeneous skin surfaces and reducing localized pressure points. Second, it improves mechanical efficiency, with tessellated geometry ensuring uniform distribution of tensile and compressive forces at the strap-brace interface. The hybrid design (foldable arc + rigid support) balances structural integrity and ergonomic performance, demonstrating the potential of origami engineering in wearable device optimization.

(2) Clarified Motion Mechanism and Ring-Forming Characteristics: By selecting the folding angle ρA1B1 as the input parameter, the study derives the correlation formulas between ρA1B1 and key parameters (Ri, L, n·x), revealing the non-linear variation laws of structural span during folding. Investigation into full folding ring formation shows that a complete ring structure inevitably

DOI: 10.54254/2755-2721/2025.GL27340

undergoes an "over-ring" stage (excessive overlap), which conflicts with dynamic adaptation requirements. Thus, adopting a semi-arc structure avoids this issue, retaining sufficient deformation freedom to fit leg curvature changes.

(3) Optimized Structural Parameters for Limb Adaptation: Through control variable experiments, the influence of core parameters (a1, a2, αI1, αI1') on crease distribution is clarified: reducing a2 increases crease density (improving conformity), while reducing αI1' decreases density (impairing comfort). Based on ergonomic constraints for the thigh and calf, optimized parameters are obtained, with their performance ranges (L: 14.62–18.56 cm for thigh, 8.46–10.99 cm for calf; Ri: 7.40–9.49 cm for thigh, 4.76–6.09 cm for calf; n·x: 182.66°–220.36° for thigh, 206.74°–248.52° for calf) all meeting design requirements, ensuring effective fit during limb movement.

(4) Validated Prototype Performance: Physical models of the thigh, calf, lockable bracket system (with U-groove and rotation mechanism), and triangular linkage are fabricated, and the overall model is assembled. The prototype demonstrates stable structural performance in validation, with no deformation during gait simulation, confirming the feasibility of the design.

In summary, this study provides a novel solution for improving knee brace ergonomics by combining origami structures with biomechanical requirements. Future work will focus on: (1) enhancing structural stability, such as optimizing anti-interference performance to reduce displacement during leg vibration and improving U-groove connection security with ratchet-lock mechanisms or memory metal; (2) developing advanced material systems (e.g., carbon fiber/PEEK composites for brackets, auxetic polyurethane foam for Miura structures) to further improve performance and reduce weight; (3) conducting clinical trials to verify long-term wearing comfort and therapeutic effects, promoting practical application.

References

[1] Wright R W, Fetzer G B. Bracing after ACL reconstruction: a systematic review [J]. Clinical Orthopaedics and Related Research®, 2007, 455: 162-168.

[2] Du Y, Keller T, Song C, et al. Design and foldability of Miura-based cylindrical origami structures [J]. Thin-Walled Structures, 2021, 159: 107311.

[3] Xiang, X. M., Guoxing Lu, Dong Ruan, Z. You, and M. Zolghadr. "Large deformation of an arc-Miura structure under quasi-static load." Composite Structures 182 (2017): 209-222.

[4] Zhang, Qian, Xinyu Wang, Daniel Sang-hoon Lee, Jianguo Cai, Zheng Ren, and Jian Feng. "Development of kinetic origami canopy using Arc Miura folding patterns." Journal of Building Engineering 43 (2021): 103116.

[5] LIANG, Y. B., CONG, G. H., ZHANG, Y. X., et al. Study on flow field performance of U-groove mechanical seal [J]. Lubrication Engineering, 2024, 49(11): 190-196.

[6] YUE, T. T. Innovative application of origami art in furniture design [J]. Shanghai Packaging, 2023, (05): 141-143. https: //doi.org/10.19446/j.cnki.1005-9423.2023.05.048

[7] XIE, N., ZHANG, Z. Y. Application of origami art in modern design [J]. Journal of Tianjin Academy of Fine Arts, 2022, (04): 89-91.